Final Technical Report

for

Multi-Stage Aeroelastic Analysis for Propulsion

Dr. Theo G. Keith, Jr.
Principal Investigator

Dr. Milind A. Bakhle
Co-Principal Investigator

Department of Mechanical, Industrial and Manufacturing Engineering
University of Toledo
Toledo, Ohio 43606

June 2003

Final Report for NASA grant NCC3-717

Multi-Stage Aeroelastic Analysis for Propulsion

by

Dr. Theo G. Keith, Jr. (Distinguished University Professor)
Dr. Milind A. Bakhle (Senior Research Associate)

University of Toledo

High-Cycle Fatigue (HCF) failure, caused by forced response vibrations, is the predominant problem in new aircraft engines. In the future, high-speed engines will have fewer turbomachinery stages with higher loadings to reduce weight. The increased interactions between compressor and turbine stages due to reduced blade row spacing will lead to increased forced vibration response problems that will result in more HCF failures. Numerical modeling is the key to understanding and avoiding such multi-stage aeroelastic problems in the design and development stage. In the future, to reduce launch costs of re-usable launch vehicles, rocket turbopumps will be built to withstand many flights before requiring major maintenance or overhauling. An accurate prediction of the unsteady loads and dynamic stresses on the blading will be necessary to correctly predict the HCF life of these turbomachinery components.

The first step in the current effort was to assess the existing capability to perform aeroelastic calculations for a turbomachinery stage. With this objective, an industry configuration was identified which had encountered aeroelastic problem during initial design. This was a high-pressure (HP) turbine that experienced high dynamic stresses in an initial design. The stresses were reduced to acceptable levels in the final design by increasing the axial gap between the vanes and rotor blades.

The TURBO-AE code was used to perform the analysis. Code modifications were made to compute the unsteady aerodynamic (pressure and viscous) forces acting on the blade surfaces. To perform the computations for this stage using periodic boundary conditions in the blade-to-blade direction would require the modeling of 41 stators passages and 78 rotor passages. It was determined that the computational resources would not be available to perform the calculation in this manner. The modeled geometry was changed to have 39 stators and 78 rotors with an appropriate scaling of the stator pitch. It was now possible to compute the unsteady flowfield using one stator passage and two rotor passages.

After the completion of these initial computations, a second effort was made to use time-shift periodic boundary conditions in a later version of the TURBO-AE code to model the unmodified geometry (41 stators and 78 rotors). With the time-shift periodic boundary conditions, it was possible to model the original unmodified HP turbine geometry with only one stator passage and one rotor passage included in the computations. The newer version of the TURBO-AE code was modified to include the computation of unsteady aerodynamic forces.

Two configurations were analyzed with different axial spacing between blade rows. Three operating conditions were analyzed corresponding to the resonant crossings of modes 2, 3, and 4 on the Campbell diagram for each of the two configurations. Flowfield visualization was done that showed the viscous wake from the upstream vanes was the source of the unsteady excitations on the rotors. The steady and unsteady blade surface pressure distributions were compared in detail with the measurements acquired by other researchers in a short duration test facility. All these results were documented in Ref. 1. As part of this work, detailed sensitivity studies were also performed to ensure that the numerical results were not unduly influenced by the choice of various numerical inputs. Also, the results obtained from the TURBO-AE code were compared with results from the UNSFLO code in collaboration with industry partners.

The next step in this effort was to combine the forcing functions, obtained in the preceding effort, with separate calculations of aerodynamic damping to determine the strain in the rotor blades. This work was done in collaboration with industry partners and the calculated blade strains were compared with measurements obtained by other researchers in the short duration facility. This work has been documented in Ref. 2.

At the conclusion of this work, the forced response calculations have been performed using the TURBO-AE code with a single turbomachinery stage being modeled. The significant computational effort required to extend these calculations with TURBO-AE to multiple blade rows can be accomplished using the parallel version of the TURBO code that has been developed by other researchers. This work will be attempted in future efforts.

References

1. "Calculation and Correlation of the Unsteady Flowfield in a High Pressure Turbine", Bakhle, M. A., Liu, J. S., Panovsky, J., Keith, T. G., Jr., and Mehmed, O., ASME Paper 2002-GT-30322, June 2002; also NASA TM-2002-211475. March 2002.

2. "Comparisons of Experimental and Computational Forced Response in a High Pressure Turbine", Panovsky, J., Liu, J. S. and Bakhle, M. A., Proceedings of the 7th National Turbine High Cycle Fatigue Conference, published by Universal Technology Corporation, Dayton, Ohio, April 2002.

Appendix

(Attach NASA TM)

Comparisons of Experimental and Computational Forced Response in a High Pressure Turbine

J. Panovsky and J. Liu, Honeywell Aerospace
Milind A. Bakhle, University of Toledo

Abstract

Forced vibrations in turbomachinery components can cause blades to crack or fail due to High Cycle Fatigue. In recent years, computational fluid dynamics (CFD) methods have become available that can model the unsteady aerodynamics which provide the driving mechanism for the vibration. However, thorough validation of these unsteady CFD codes is required before they can be relied on for production design analysis. In this paper, predictions from the CFD code TURBO are compared to experimental results for a high pressure turbine blade excited by the upstream vane. TURBO is a 3D, unsteady, multiple blade row Navier-Stokes code developed at Mississippi State University. The test data was generated in the Gas Turbine Laboratory at Ohio State University through a GUIde Consortium project. The turbine blade of interest experienced high vibratory strains until a re-design effort increased the axial spacing between the vane and the blade. The results presented include comparisons of unsteady pressure on the blade surface as well as vibratory response levels at two axial spacings for several modes encountered. Predictions of aero damping for these modes are also compared to measurements made during the forced response tests.

Introduction

High Cycle Fatigue (HCF) continues to be a significant problem in gas turbine engines, and forced response vibrations due to unsteady aerodynamic excitations from adjacent blade rows are a major cause of blade failures. Modern turbomachinery blade designs have higher pressure ratios and smaller axial gap between blade rows, which can cause an increase in forced response problems. These problems, which are often not discovered until late in the engine development cycle, can adversely affect the development cost, maintenance cost, and durability of gas turbine engines. In addition, the safety and readiness of aircraft can be compromised by HCF problems related to forced response in aircraft engines.

1

As an example of forced response in actual engines, the high-pressure turbine blades in a small turbofan engine had an unexpectedly high failure rate in early production. The cause of these failures was identified as forced response resulting from the vortical excitations from vane wakes. The vane count resulted in the excitation of the 2nd torsion mode in the operating range. The problem was remedied by increasing the axial spacing between the stator and the rotor from 32% to 46% of axial chord. This change led to a 50% reduction in the vibratory strain and the engine with the modified high-pressure turbine stage is widely used in business jet applications today without any safety or durability concerns.

Although the Campbell diagram can identify regions of potential problems, the actual magnitude of the aerodynamic excitation and the resulting blade vibratory response can only be obtained from experimental testing or unsteady aerodynamic and structural modeling. Without such information, it is impossible to determine whether a particular crossing on the Campbell diagram will result in problems. With recent advances in CFD modeling techniques and increased availability of computational resources, it is now possible to model a turbine stage in considerable detail. Such modeling, which includes three dimensional and viscous effects, can provide details of the unsteady flow phenomena and yield the aerodynamic excitation to calculate the blade vibratory response. However, validation of such CFD-based models requires unsteady aerodynamic and vibration response data.

The turbine stage mentioned previously was recently tested in a short duration test facility (shock tunnel) in the Gas Turbine Laboratory at the Ohio State University under a contract from the GUIde Consortium (Kielb et al., 2001a, 2001b). The acquired data includes measurements of the unsteady pressure on the blade surfaces and the vibratory strain of the blades due to excitations from upstream vanes at various operating speeds and conditions. The data set includes measurements at two different axial gaps between the stator and the rotor. In addition, separate testing using piezoelectric actuators was done in vacuum to measure the mechanical damping present. Unfortunately, an irrecoverable loss of the on-blade instrumentation occurred before unsteady pressure data could be acquired for the 2nd torsion mode that encountered the forced response problem in the engine. However, data was acquired for several of the lower frequency modes, and this benchmark data set is suitable for validation of unsteady aerodynamics and aeroelastic analysis codes.

Forced Response Correlations

The TURBO code originally developed by Janus et al. (1989a, b) and Chen (1991, 1993) at Mississippi State University is used for the present study. It is a three-dimensional, unsteady, Reynolds-averaged, Navier-Stokes solver for modeling the flow through multistage turbomachinery. The code is based on an implicit finite volume algorithm. A total variation diminishing (TVD) scheme is used to evaluate the fluxes and Newton sub-iterations are used at each time step to maintain high accuracy. A two-equation k-ε turbulence model is used for closure. Phase-lag boundary conditions, based on the direct-

store method (Erdos et al., 1977) have been implemented in the TURBO code by Chen et al. (1994), and these were utilized for the unequal blade count between the stator and rotor.

Bakhle et al. (1996, 1997) developed routines to include the structural deflections in the TURBO solver. These routines indirectly couple three-dimensional fluid and structural dynamic models to permit flutter and aerodynamic damping analyses. This feature, however, is available for single-blade-row analyses only. The computations presented in this paper were conducted by utilizing two-blade-row solutions to determine the excitation forces, and separate single-blade-row analyses to determine the aero damping.

For the high pressure turbine stage used in the present study, the upstream stator has 41 vanes and the downstream rotor has 78 blades (Figure 1). A representative computational grid, consisting of an H-grid smoothed by a Poisson solver, is shown in Figure 2. The stator and rotor grids are 95x43x37 (axial x radial x circumferential) and 93x43x37, respectively. For clarity, Figure 2 shows the grids in multiple passages; the computational domain actually includes only a single passage in each blade row.

Unsteady flow solutions are obtained for two different axial spacings between the stator and rotor: 32% and 46% of stator chord, referred to as the small and large gap. Three modes including mode 2 (first torsion, 1T), mode 3 (axial, 1A), and mode 4 (second bending, 2B) are analyzed in this study. Table 1 provides a summary of conditions for the TURBO analyses. In Bakhle et al. (2002), the present authors discuss in detail the results from the unsteady aerodynamic analyses and present comparisons of the unsteady pressure to measured values. Figure 3 provides a typical example of the correlation for reference. The predicted and measured unsteady pressures are seen to be in fairly good agreement, though some discrepancies can be noted. Additional comparisons can be found in the previously cited reference. The primary focus of the present paper is the comparison of vibratory strains.

Once the unsteady pressures have been calculated by TURBO, the vibratory strains can be obtained by utilizing the mode shapes from a finite element model and values for the damping. In the present case, a modal approach is employed where the product of the unsteady pressures and the mode shape produce a modal force. This modal force is then used in conjunction with the standard equations for a single-degree-of-freedom system to determine the modal amplitude at resonance. This modal amplitude becomes a scaling factor to be applied to the finite element results to determine the physical vibratory strain distribution. Use of a single-degree-of-freedom approach is justified since the modes are well separated and the damping is small.

Sample results are shown in Figure 4, which summarizes predictions on the suction surface of the blade for mode 2 (1T) and mode 4 (2B). The plots provide the magnitude of the first Fourier harmonic of the unsteady pressure, the magnitude of the modal displacement (mode shape), and the magnitude of the first Fourier harmonic of the modal force distribution. It is evident that there is a significant change in the unsteady pressures for these two cases. The cases were run at different inlet pressures, and are at signifi-

cantly different speeds and frequencies (refer to Table 1). The combination of the change in unsteady pressures and different mode shapes provide drastically different distributions of modal forces.

This modal force distribution is integrated over each surface of the blade, and the result is used to determine the vibratory strains. For the initial calculations, the measured value of total damping was used for the predictions. Figure 5 is a comparison of the measured and predicted magnitude of the first Fourier harmonic of strain at each of the strain gage locations (hub, midspan, and tip). The first item to note is that the measured strains for all modes is extremely small, even though these cases correspond to the small axial gap. Typical failure levels of vibratory strain are on the order of 1000 μ-in/in, and any level below 100 μ-in/in is usually considered to be "in the noise". Unfortunately, all of the measured strains are well below this value. Kielb et al. (2001a, 2001b) discuss this issue in some detail and conclude that the signal-to-noise ratio in the measurements is adequate.

Despite this concern, the predicted strains agree fairly well with the measurements overall. Modes 2 and 3 are predicted to have extremely small responses, which is in accordance with the measurements. The measured response in mode 4 is significantly larger, and this increased response level is also predicted. The direct comparison of the measured and predicted strains is quite good at the tip and midspan gages for all of the modes. There is a substantially larger discrepancy at the hub gage, with the measurement consistently much lower than the prediction for each mode. This discrepancy could arise from many sources, but the most likely cause is the hub gage being located in the high strain gradient region associated with the airfoil root fillet. Other potential causes include mislocation of the gage (either in the test or the analysis), significant blade-to-blade variations in amplitude or mode shape, or changes in the mode shapes due to the blade modifications needed to accommodate the instrumentation. Further investigation is needed to resolve this fundamental discrepancy.

In another portion of the experimental investigation, Kielb et al. (2001a) note a surprising trend in that the vibratory strains for mode 4 actually increase as the axial gap is increased. This result is opposite to intuition, and also to the behavior for the other modes. However, this behavior is corroborated by predictions from TURBO. The results, summarized in Figure 6, indicate very good agreement at the highest-reading midspan gage location. Plots similar to those shown in Figure 4 indicate that, while the overall unsteady pressures decrease significantly with the increase in axial gap, phasing effects cause the net modal force to increase.

Damping Correlations

The predicted strains presented up to this point have utilized predicted values for the excitation force, but the damping values were based on those measured during the rig tests. We also want to assess the ability to predict the damping levels observed, and to conduct forced response assessments based completely on calculated values. During the rig tests, a series of tests were conducted using piezoelectric actuators to force individual blade

vibration (Kielb et al., 2001a). Because these tests were conducted in vacuum, the primary contributor to damping is structural; in particular, the friction damping at the dovetail (there are no under-platform dampers).

The damping measurements for these in-vacuum tests can be compared to those run in air during the forced response tests. The damping measured during the tests in air contains contributions from both aero and friction damping; as usual, material damping is assumed to be negligibly small. Since both sets of tests were run at vibration amplitudes of the same order of magnitude, we can assume that the individual contributions to total damping remain constant. Therefore, the structural or friction damping is defined to be that obtained from the in-vacuum tests, while aero damping is defined as the difference of the in-air test and the friction damping. Each of these damping values was determined separately for each mode based on averaging the available strain gage values presented in Kielb et al. (2001a, 2001b). Measured results are only available for modes 2 and 4, and the damping values are presented in Table 2.

TURBO is then used to predict values for the aero damping for a 41 nodal diameter backward-traveling wave. The results are summarized in Table 2 and also in Figure 7. The predicted values are significantly below the measurements for both modes where values are available. It is worth noting, though, that even the predicted values indicate that the aero damping is the primary contributor to the total damping, in agreement with the experimental results.

One potential cause for the large discrepancy between the measured and predicted aero damping values is that the rig test rotor did not behave as a tuned system mode (Kielb, 2002), as assumed in the TURBO analysis. Because of the small size of the blades, the instrumentation and piezoelectric actuators caused a significant change in the blade frequencies. As a result, the rotor behavior was much closer to individual blade resonances than a tuned system response. To assess the impact on the predictions, each mode was run through the full range of nodal diameters, with the results summarized in Figure 8. Using the notion of influence coefficients (Crawley, 1988), this result was Fourier transformed to obtain the reference blade contribution. This contribution corresponds to the blade self-damping term and should be a good approximation to the behavior of the rotor as described. However, due to the small changes in damping that occur over the nodal diameter range, we found that this value was not significantly different than the tuned value for 41 nodal diameter. See Figure 9 for a direct comparison.

The vibratory strains were then predicted using the excitation forces calculated by the coupled forced response analysis, the predicted aero damping, and the measured friction damping. The aero damping values corresponding to 41 nodal diameter were used. The results are compared to the measurements in Figure 10. Given the discrepancies in the damping predictions, it is not surprising that the reasonably good correlation presented in Figure 5 has deteriorated considerably. It is obvious that continuing work is needed to resolve these inconsistencies in the damping.

Summary and Conclusions

Overall, the predicted vibratory strains are in fairly good agreement with the measurements as long as the measured damping values are used. This indicates that the predictions of the excitation forces are reasonably accurate. However, significant discrepancies occur in the predictions of aero damping, which are off by a factor of approximately 3 to 4. This causes a corresponding change in the predicted vibratory strain when the predicted damping is utilized. Perhaps most importantly the analysis -- regardless of the precise assumption for damping -- predicts that the response in each of these modes should be very small, as verified by the rig testing. It is extremely unfortunate that the instrumentation was lost in the rig before the mode that has demonstrated large responses in the engine could be reached. The extremely low vibratory responses of the rig tests do raise concerns in their use for code validation purposes. The low responses bring another level of complexity to the already extremely challenging task of obtaining on-blade measurements. However, the research lab has investigated this issue and concluded that the signal-to-noise ratio is adequate.

We found that the measured and predicted strains, when using the measured damping values, correlated well at the tip and midspan gage locations but there were sizable differences at the hub gage. This appears to indicate that there is a difference in the relative strain readings between the rig tests and the corresponding finite element model for each mode, which is likely due to the gage being located in a high strain gradient region near the airfoil root fillet. This discrepancy must be resolved before an improvement to the correlation can be attained.

The work presented in this paper is part of an overall correlation effort to determine the capabilities of the TURBO code to predict flutter and forced response. The work is in the early stages, and the results presented here should be taken as a current status of initial results rather than a final conclusion. The main purpose of conducting these validation efforts is to identify areas that need improvement, either in the modeling approach or in the code itself. The results of this study should be helpful in guiding future development in both modeling and code enhancements.

There is still a significant amount of raw data remaining from the series of rig tests that have yet to be fully reduced and analyzed, consisting primarily of strain gage data for those cases not presented here. The authors of this paper encourage further data reduction and analysis of the measurements so that the results of this important and unique experimental effort can be fully exploited.

Acknowledgements

References

Bakhle, M.A., Srivastava, R., Stefko, G.L., and Janus, J.M., "Development of an Aeroelastic Code Based on an Euler/Navier-Stokes Aerodynamic Solver," ASME Paper 96-GT-311, 1996.

Bakhle, M.A., Srivastava, R., and Keith, T.G. Jr., "A 3D Euler/Navier-Stokes Aeroelastic Code for Propulsion Applications," AIAA Paper 97-2749, July, 1997.

Bakhle, M.A., Liu, J.S., Panovsky, J., Keith, T.G. Jr., and Mehmed, O., "Calculation and Correlation of the Unsteady Flowfield in a High Pressure Turbine," ASME Paper GT-2002-30322, 2002.

Chen, J.P., "Unsteady Three-Dimensional Thin-Layer Navier-Stokes Solutions for Turbomachinery in Transonic Flow," Ph.D. Dissertation, Mississippi State University, 1991.

Chen, J.P., and Whitfield, D.L., "Navier-Stokes Calculations for the Unsteady Flowfield of Turbomachinery," AIAA Paper 93-0676, January, 1993.

Chen, J.P., Celestina, M., and Adamczyk, J.J., "A New Procedure for Simulating Unsteady Flows through Turbomachinery Blade Passage," ASME Paper 94-GT-151, 1994.

Crawley, E.F., "Aeroelastic Formulation for Tuned and Mistuned Rotors," Chapter 19 in AGARD Manual on Aeroelasticity in Axial-Flow Turbomachines, Vol. 2, Structural Dynamics and Aeroelasticity, M.F. Platzer and F.O. Carta, eds., AGARD-AG-298, 1988.

Erdos, J.I., Alzner, E., and McNally, W., "Numerical Solution of Periodic Transonic Flow Through a Fan Stage," AIAA Journal, Vol. 15, pp. 1559-1568, 1977.

Janus, J.M., "Advanced 3-D CFD Algorithm for Turbomachinery," Ph.D. Dissertation, Mississippi State University, 1989.

Janus, J.M., and Whitfield, D.L., "A Simple Time-Accurate Turbomachinery Algorithm with Numerical Solutions of an Uneven Blade Count Configuration," AIAA Paper 89-0206, January, 1989.

Kielb, J.J, and Abhari, R.S., "Experimental Study of Aerodynamic and Structural Damping in a Full-Scale Rotating Turbine," ASME Paper 2001-GT-0262, 2001.

Kielb, J.J, Abhari, R.S., and Dunn, M.G., "Experimental and Numerical Study of Forced Response in a Full-Scale Rotating Turbine," ASME Paper 2001-GT-0263, 2001.
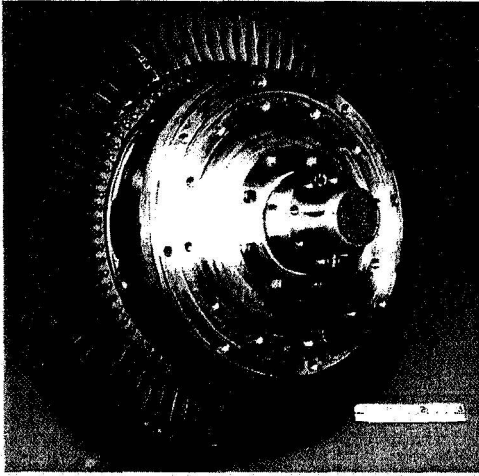
Kielb, J.J., personal communication, 2002.

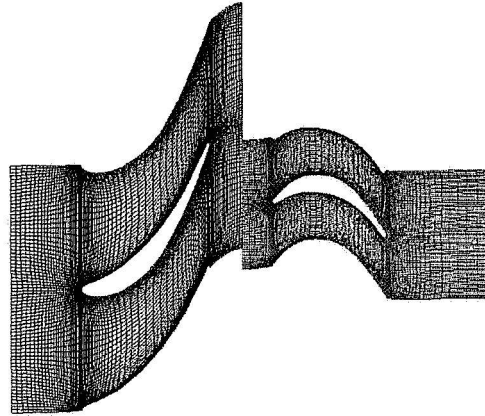**Figure 1.** High pressure turbine rotor used in study.

Figure 2. Grid used for unsteady aero computations.

Run	Mode	Rotational Speed (RPM)	Frequency (Hz)	Inlet Pressure (Pa)	Inlet Temp (K)	Pressure Ratio	Axial Spacing
7	2 (1T)	10100	6900	289590	296	1.6	32%
14	2 (1T)	10100	6900	289590	296	1.6	46%
1	3 (1A)	15000	11100	289590	296	2.1	32%
11	3 (1A)	15000	11100	289590	296	2.0	46%
4	4 (2B)	19500	13300	558495	553	2.1	32%
16	4 (2B)	19500	13300	565390	553	2.1	46%

Table 1. Summary of conditions used in TURBO calculations.
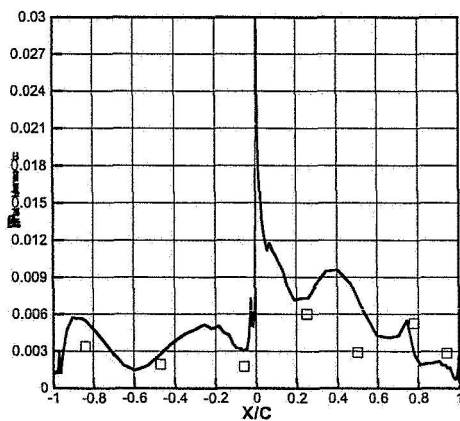
(a) Run 7 conditions, 1st harmonic magnitude
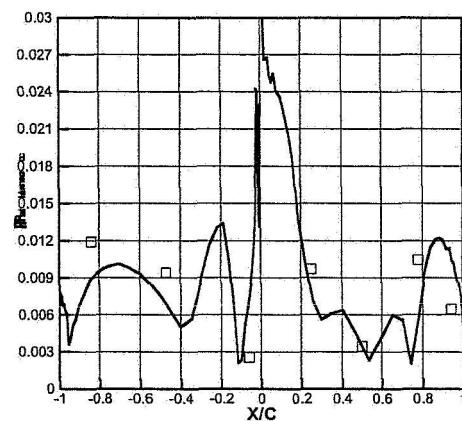
(b) Run 4 conditions, 1st harmonic magnitude

Figure 3. Example of correlation of predicted and measured unsteady pressures.

Unsteady Pressure, 1st Harmonic Magnitude
(a) Mode 2   (b) Mode 4

Mode Shape Magnitude
(c) Mode 2   (d) Mode 4

Modal Force, 1st Harmonic Magnitude
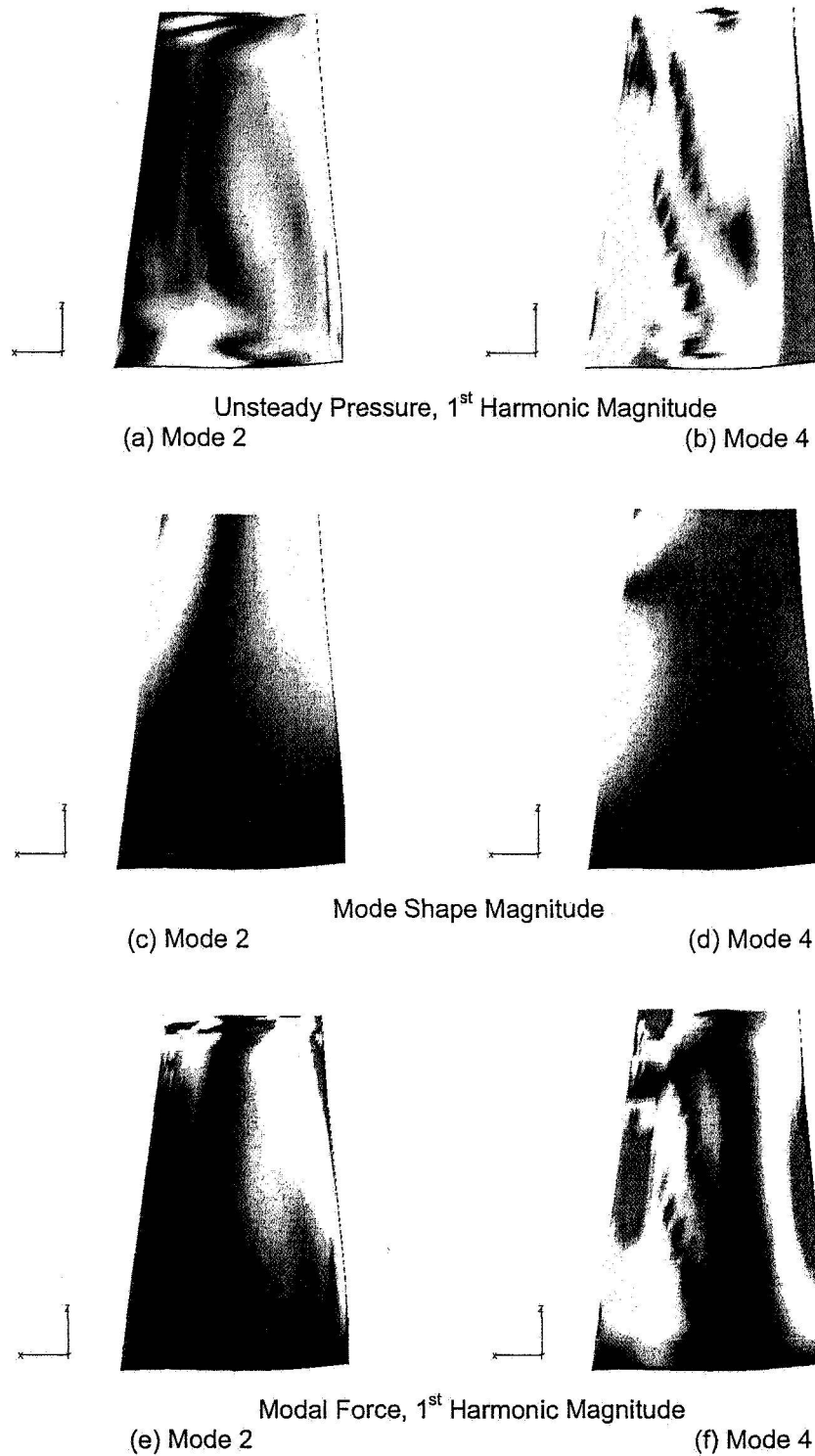(e) Mode 2   (f) Mode 4

Figure 4. Distributions of unsteady quantities for Mode 2 (1T) and Mode 4 (2B). The suction surface is shown in each plot, with the LE to the right. Blue indicates a value of zero, while red regions are the maximum.
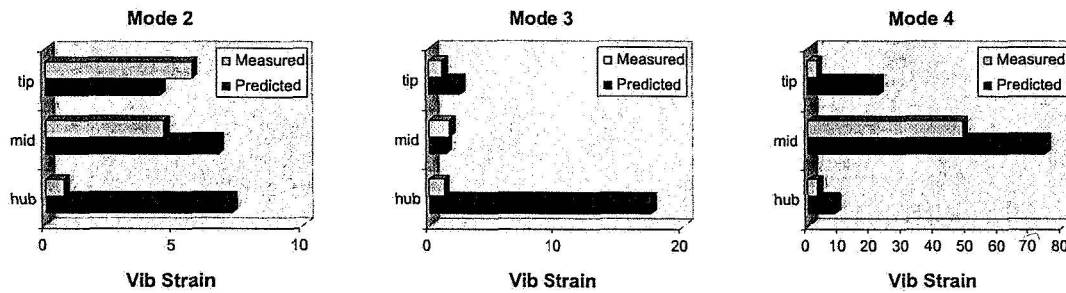
Figure 5. Comparison of measured and predicted vibratory strains (μ-in/in). The predicted values were obtained by using the calculated unsteady forces and the measured total damping.
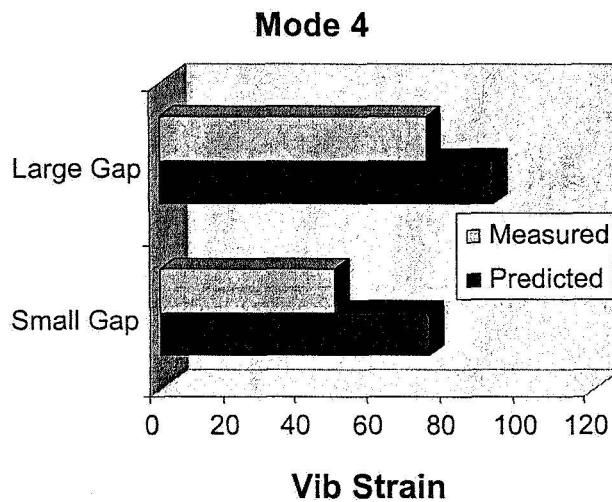

Figure 6. Change in Mode 4 (2B) response level (μ-in/in) with increased axial gap.

Damping	Mode 2		Mode 4	
	Measured	Predicted	Measured	Predicted
Aero	1.09 ± 0.49	0.25	0.35 ± 0.09	0.12
Friction	0.12 ± 0.01	0.12	0.09 ± 0.01	0.09
Total	1.21 ± 0.50	0.37	0.44 ± 0.10	0.21

Table 2. Comparison of measured and predicted damping levels (ζ%).
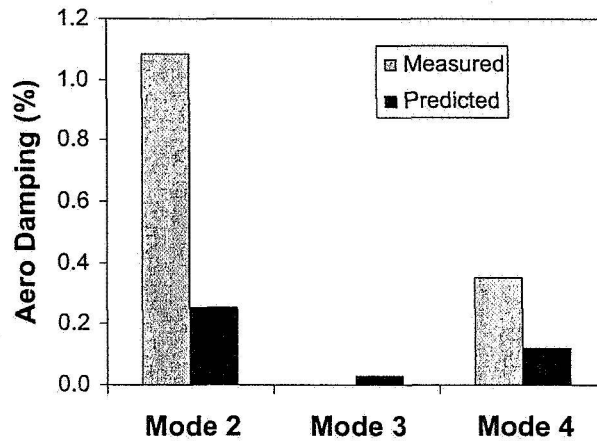
Figure 7. Comparison of measured and predicted aero damping levels.
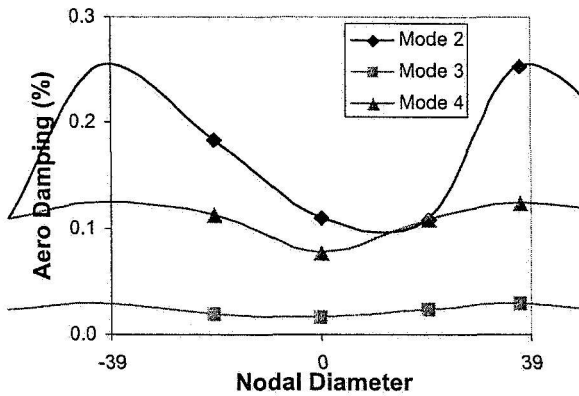

Figure 8. Variation in aero damping through entire nodal diameter range for all three modes.
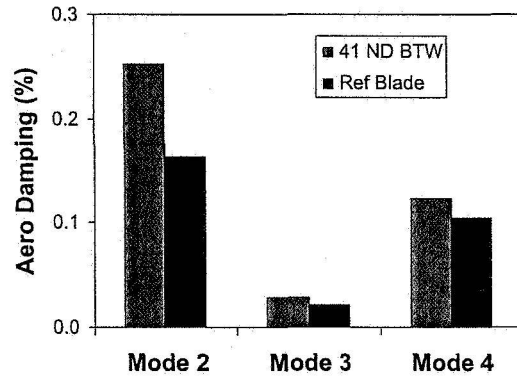

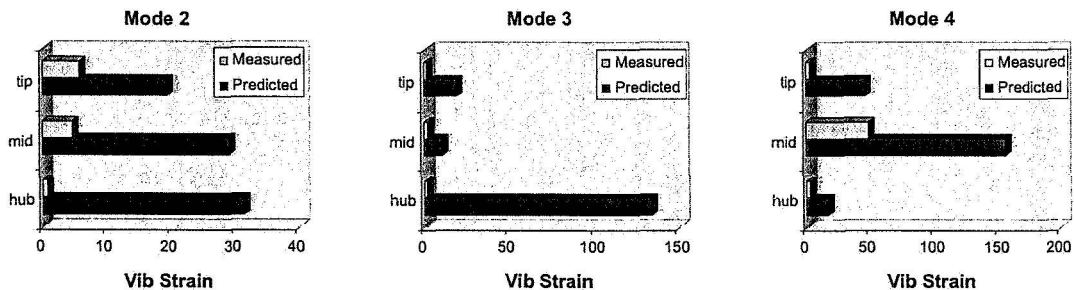**Figure 9.** Aero damping comparison for 41 nodal diameter backward-traveling wave and reference blade contribution.

Figure 10. Comparison of measured and predicted vibratory strains (μ-in/in). The predicted values were obtained by using the calculated unsteady forces and aero damping with the measured friction damping.